# New Pyrrole Inhibitors of Monoamine Oxidase: Synthesis, Biological Evaluation, and Structural Determinants of MAO-A and MAO-B Selectivity

Giuseppe La Regina,[†] Romano Silvestri,*[,†] Marino Artico,[†] Antonio Lavecchia,*[,‡] Ettore Novellino,[‡] Olivia Befani,[§] Paola Turini,[§] and Enzo Agostinelli[§]

*Dipartimento di Studi Farmaceutici, Università di Roma "La Sapienza", Piazzale Aldo Moro 5, I-00185 Roma, Italy, Dipartimento di Chimica Farmaceutica e Tossicologica, Università degli Studi di Napoli "Federico II", Via Domenico Montesano 49, I-80131 Napoli, Italy, and Dipartimento di Scienze Biochimiche "Rossi Fanelli" and Istituti di Biologia e Patologia Molecolare del CNR, Università di Roma "La Sapienza", Piazzale Aldo Moro 5, I-00185 Roma, Italy*

*Received July 26, 2006*

A series of new pyrrole derivatives have been synthesized and evaluated for their monoamine oxidase (MAO) A and B inhibitory activity and selectivity. *N*-Methyl,*N*-(benzyl),*N*-(pyrrol-2-ylmethyl)amine (**7**) and *N*-(2-benzyl),*N*-(1-methylpyrrol-2-ylmethyl)amine (**18**) were the most selective MAO-B (**7**, SI = 0.0057) and MAO-A (**18**, SI = 12500) inhibitors, respectively. Docking and molecular dynamics simulations gave structural insights into the MAO-A and MAO-B selectivity. Compound **18** forms an H-bond with Gln215 through its protonated amino group into the MAO-A binding site. This H-bond is absent in the **7**/MAO-A complex. In contrast, compound **7** places its phenyl ring into an aromatic cage of the MAO-B binding pocket, where it forms charge-transfer interactions. The slightly different binding pose of **18** into the MAO-B active site seems to be forced by a bulkier Tyr residue, which replaces a smaller Ile residue present in MAO-A.

## Introduction

Amine oxidases (amine: oxygen oxidoreductases, AOs) are a heterogeneous superfamily of enzymes that catalyze the oxidative deamination of mono-, di-, and polyamines. AOs differ because of their molecular architecture, catalytic mechanisms, and subcellular localizations. On the basis of the chemical nature of the cofactor, AOs fall into two classes: FAD−AOs (EC 1.4.3.4) and Cu/TPQ−AOs (1.4.3.6)1. Both classes have been isolated and characterized from micro-organisms, plants, and mammals. FAD−AOs are mainly intracellular enzymes and are often associated with the outer mitochondrial membrane.[1]

The isoforms MAO-A and MAO-B have been described on the basis of their substrate and inhibitor specificity.[2,3] MAO-A catalyzes the oxidative deamination of serotonin (5-HT), adrenaline (A), and noradrenaline (NA) and is selectively inhibited by clorgyline (**1**) and moclobemide (**2**) (Chart 1). MAO-B catalyzes the oxidative deamination of $\beta$-phenetylamine and benzylamine and is selectively inhibited by selegiline (**3**). Both isoenzymes deaminate dopamine (DA) in vitro and tyramine, but human DA is preferentially metabolized by MAO-B. Compounds **1** and **3** are irreversible inhibitors, whereas **2** is a reversible MAO inhibitor. The kinetic aspects as well as the possible functions of MAOs have been recently reviewed by Tipton.[4]

MAO-A and MAO-B have essential roles in vital physiological processes and are involved in the pathogenesis of various human diseases. The MAO inhibitors are used for the treatment of psychiatric and neurological disorders.[5,6] MAO-A inhibitors are prescribed for mental depression. MAO-B inhibitors are used in Parkinson's disease (PD), a neurodegenerative syndrome for which the main therapy is the amelioration of symptoms with L-DOPA and/or DA agonists.[7] MAO-B is also involved in the apoptotic process. At high concentrations, selegiline combined with L-DOPA induces neuronal apoptosis, whereas at lower concentration is a neuroprotector agent that prevents from the apoptotic event.[8] PF 9601N was recently discovered as an irreversible MAO-B inhibitor that attenuates MPTP-induced depletion of striatal dopamine levels in C57/BL6 mice.[9] The anti-MAO-B activity of the adenosine $A_{2A}$ receptor antagonist KW-6002 may ameliorate its neuroprotective activity in anti-PD therapy.[10]

We previously reported the synthesis of simple and highly selective pyrrole MAO-A and MAO-B inhibitors. This new class of MAO inhibitors was designed using a reference model that we developed starting from the structures **2** and **3** (Chart 1).[11] *N*-Methyl,*N*-propargyl,*N*-(pyrrol-2-ylmethyl)amine (**4**) was a potent, although not selective, MAO-A inhibitor ($K_i$ = 0.0054 $\mu$M). The pyrrole-2-carboxyamides **5** an **6** showed high selectivity for the MAO-A (SIs = 2025 and >2500, respectively; the selectivity index (SI) was calculated as $K_i$(MAO-B)/$K_i$(MAO-A) ratio, and *N*-methyl,*N*-benzyl,*N*-(pyrrol-2-ylmethyl)amine (**7**) was highly selective for the B isoenzyme (SI = 0.0057).[11] These results prompted us to synthesize new pyrrole analogues (**8**−**36**) in order to extend the structure−activity relationship (SAR) study. To investigate the structural determinants of MAO-A/B selectivity, we carried out docking studies and molecular dynamics (MD) simulations of the most selective inhibitors **7** and **18**.

**Chemistry.** The pyrrole-2-carboxamides **8**, **11**−**16**, **24**, **27**, **28**, **32**, and **33** were obtained in good yield by heating 2-trichloroacetyl-1*H*-pyrrole[12] at 60 °C with appropriate amines in the presence of triethylamine (Scheme 1). However, by use of either *N*-methyl-α-phenylethylamine or *N*-methyl-α-cyclohexylamine, this reaction produced a poor yield. To improve the yield, we synthesized the amides **25**, **29**, and **30** using pyrrole-2-carboxylic acid in the presence of (benzotriazol-1-

* To whom correspondence should be addressed. Phone: +39 06 4991 3800 (R.S.); +39 081 678 613 (A.L.). Fax: +39 06 491 491 (R.S.); +39 081 678 613 (A.L.). E-mail: romano.silvestri@uniroma1.it (R.S.); lavecchi@unina.it (A.L.).

[†] Dipartimento di Studi Farmaceutici.

[‡] Dipartimento di Chimica Farmaceutica e Tossicologica.

[§] Dipartimento di Scienze Biochimiche "Rossi Fanelli" and Istituti di Biologia e Patologia Molecolare del CNR.

10.1021/jm060882y CCC: $37.00 
Published on Web 01/26/2007

**Chart 1.** Structures of Reference and New Pyrrole Inhibitors of Monoamine Oxidase

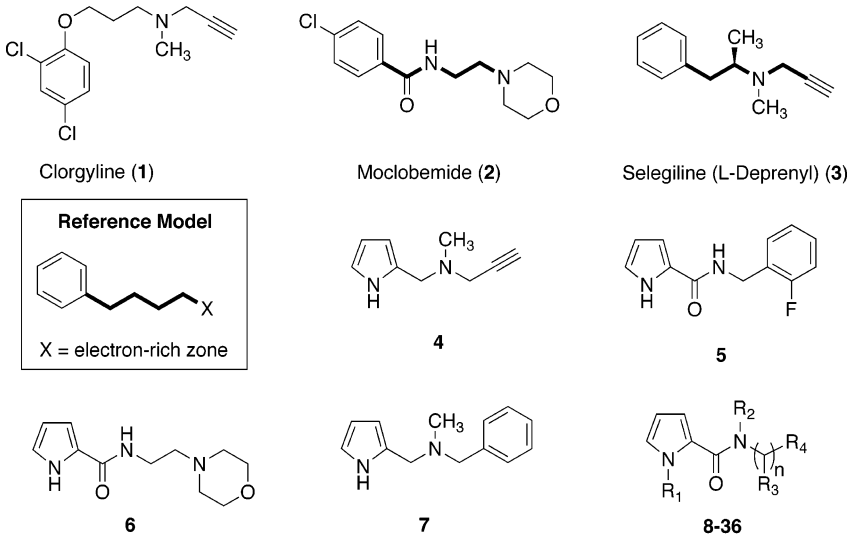


**Scheme 1.** Synthesis of Pyrrole-2-carboxamides **8**, **11**−**16**, **24**, **25**, **27**−**30**, and **32**−**34**[a]

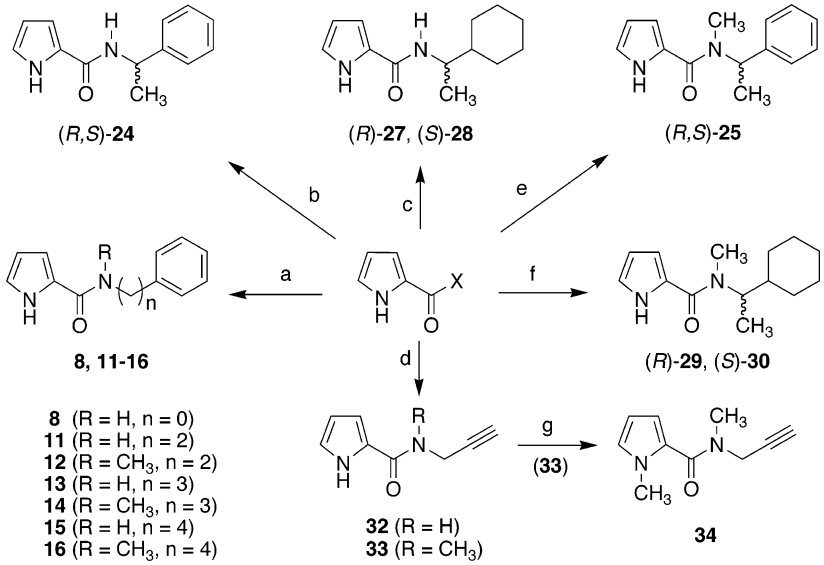


[a] Reagents and Reaction Conditions. (a-d) X═$CCl_3$, amine, $Et_3N$, 60 °C, overnight. Amine: (a) Benzylamine or *N*-methylbenzylamine, (b) (*R,S*)-α-phenylethylamine, (c) (*R*)-α-cyclohexylethylamine or (*S*)-α-cyclohexylethylamine, (d) Propargylamine or *N*-methylpropargylamine. (e, f) X═OH, amine, BOP, $Et_3N$, DMF, room temperature, overnight; Amine: (e) (*R,S*)-*N*-methyl-α-phenylethylamine, (f) (*R*)-*N*-methyl-α-cyclohexylethylamine or (*S*)-*N*-methyl-α-cyclohexylethylamine. (g) $CH_3I$, TBAHS, 50% NaOH/$CH_2Cl_2$, room temperature, overnight.

yloxy)tris(dimethylamino)phosphonium hexafluorophosphate (BOP) reagent and trietylamine in anhydrous dimethyl formamide (DMF) at room temperature overnight. Compound **33** was methylated at position 1 with iodomethane via a phase-transfer reaction in the presence of tetrabutylammoniun hydrogen sulfate in 50% NaOH/dichloromethame to furnish **34**.

The (pyrrol-2-ylmethyl)amines **19, 21**−**23, 26, 31**, and **36** were synthesized by a reaction of pyrrole with appropriate amines in the presence of 37% formaldehyde at 0 °C for 30 min (Scheme 2). Compounds **17** and **20** were prepared by $NaBH_3CN$ reduction of the corresponding (pyrrol-2-ylmethylen)amines in THF/isopropanol at room temperature for 10 min in acidic medium. The intermediates methylenamines were obtained by heating pyrrole-2-carboxyaldehyde with the proper amine at 50 °C for 1 h. Similarly, compound **35** was obtained by reduction of the corresponding methylenamine; the $NaBH_4$ reduction in methanol at 0 °C for 30 min produced a good yield. Compound **18** was prepared by a two-step procedure without isolation of the intermediate methylenamine. Accordingly, benzylamine was added to a solution of 1-methylpyrrole-2-carboxaldehyde, and then this mixture was treated with $NaBH_3$-CN in 6 N HCl/ methanol at room temperature overnight.

**Biology.** Bovine brain mitochondria isolated according to Basford[13] were used as a source of the two MAO isoforms. The new pyrrole analogues were tested in comparison with moclobemide (MCL), clorgyline (CLG), and selegiline (SLG) as reference drugs. MAO-A and MAO-B activity was determined by a fluorometric assay, using kinuramine as a substrate, in the presence of their specific inhibitors (L-deprenyl 1 $\mu$M for MAO-A and clorgyline 1 $\mu$M for MAO-B).[14] The four final concentrations ranged from 5 $\mu$M to 0.1 mM. Dixon plots showed that the inhibition was not competitive. The inhibitory activity ($K_i$) and A selectivity (SI) of compounds **4** and **7**−**36** are summarized in Table 1. All compounds were reversible inhibitors. In fact, 95−100% of enzyme activity was restored only by dialysis after 24 h (the dialysis was performed in a

**Scheme 2.** Synthesis of Pyrrole-2-ylmethylamines **17**−**23**, **26**, **31**, **35**, and **36**[a]

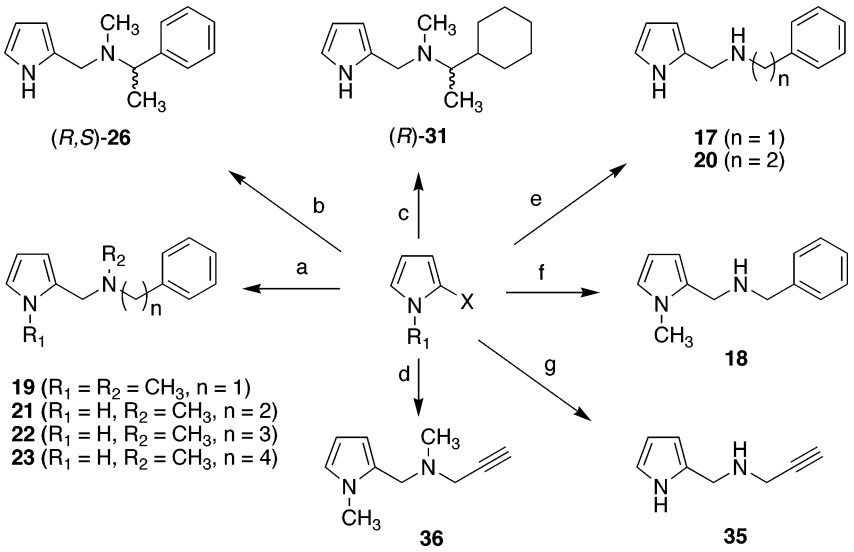


[a] Reagents and Reaction Conditions. (a-d) X═H, $R_1$═H, $CH_3$, amine, 37% HCHO, $CH_3CN$, 0 °C, 30 min. Amine: (a) Benzylamine or *N*-methylphenylalkylamines, (b) (*R,S*)-*N*-methyl-α-phenylethylamine, (c) (*R*)-*N*-methyl-α-cyclohexylethylamine, (d) *N*-methylpropargylamine, (e) X═CHO, $R_1$═H, (i) Amine, 50 °C, 1 h, (ii) $NaBH_3CN$, 1N HCl, THF, *i*-PrOH, room temperature, 10 min; (f) X═CHO, $R_1$═$CH_3$, Benzylamine, $NaBH_3CN$, 6 N HCl, THF, MeOH, room temperature, overnight; (g) X═CHO, $R_1$═H, (i) Propargylamine, THF, room temperature, 24 h, molecular sieves, (ii) $NaBH_4$, MeOH, 0 °C, 30 min.

cold room in the presence of 0.1 M potassium phosphate buffer at pH 7.2). Because of the high affinity of the inhibitors, no dissociation of the enzyme−inhibitor complex was detected during the activity assay, and the inhibition was apparently irreversible. In these experimental conditions the substrate did not compete with the inhibitor. Accordingly, a decrease of $V_{max}$ was observed, while the $K_m$ value was unchanged.

## Results and Discussion

With the only exception of **7** and **24**, tested derivatives inhibited the MAO-A at sub-micromolar concentration. Six compounds (**7**, **12**, **20**, **29**, **35**, and **36**) inhibited the B isoform in the sub-micromolar range of concentration (several derivatives inhibited the MAO-B at micromolar concentration). SI values ranged from 12 500 (**18**) to 0.0057 (**7**). The amides **12** and **29** showed the greatest MAO-A inhibitory activity ($K_i$(MAO-A) = 0.007 and 0.0017 $\mu$M, respectively). Compound **18** was the most selective MAO-A inhibitor ($K_i$(MAO-A) = 0.024 $\mu$M, $K_i$-(MAO-B) = 300 $\mu$M, SI = 12 500). Compound **29** was almost 31 times more potent than clorgyline; however, because of its potent MAO-B inhibitory activity ($K_i$(MAO-B) = 0.03 $\mu$M), it was not selective. Compounds **12**, **20**, **29**, **35**, and **36** were potent but poor selective MAO-B inhibitors.

Structure−activity relationships (SARs) were inferred from data of enzymatic experiments reported in Table 1. First we analyzed how the length of the linker group affected the anti-MAO activity (Chart 2). *N*-Phenyl-1*H*-pyrrole-2-carboxamide (**8**, $n = 0$, $K_i = 0.4$ $\mu$M) inhibited the MAO-A at a concentration 1.6 times higher than that obtained with **9** ($n = 1$, $K_i = 0.25$ $\mu$M).[11] Elongation of the alkyl chain ($n = 2, 3$) produced slight decreases of MAO-A inhibition. In contrast, **15** ($n = 4$) was 4.5 times more potent than **9** (compare **9** with **8**, **11**, **13**, and **15**). *N*-Methylcarboxamides **10** ($n = 1$) and **16** ($n = 4$) were 2.4 and 1.6 times less active than the parent compounds **9** and **15**, respectively. Conversely, compounds **12** ($n = 2$) and **14** ($n = 3$) were almost 60 and 17 times more active than **11** and **13** (compare compounds **9**, **11**, **13**, and **15** with **10**, **12**, **13**, and **16**). As MAO-B inhibitors, the *N*-methylcarboxamides were more potent than the unmethylated counterparts (compare compounds **9**, **11**, **13**, and **15** with **10**, **12**, **13**, and **16**). Great improvement of the MAO-B inhibitory activity was obtained by replacing the methylene ($n = 1$) of **10** with an ethylene group ($n = 2$) (compound **12** that was 2500 times more active than **10**). Further elongation of the linker group ($n = 3$ or 4) caused abatement of activity (compare **12** with **13**−**16**).

Reduction of unmethylated carboxamides to the corresponding amines did not affect the MAO-A inhibitory activity; the only exception were those compounds bearing the ethylene linker group (**20** was 21 times more potent than **11**; compare **9**−**12**, **14**, and **16** with **7**, **17**, and **20**−**23**). Reduction of **10** produced **7**, a compound endowed with high MAO-B inhibitory activity and selectivity.[11] Derivatives **17**−**23** were surprisingly weak MAO-B inhibitors, with the only exception being **20** ($K_i$-(MAOB) = 0.7 $\mu$M). It was clearly evident that the MAO-B selectivity was strongly associated with the presence of the *N*-benzyl,*N*-methylamino group.

As an MAO-A inhibitor, **18** was 140 times more potent than the parent compound **17** and displayed high selectivity (SI = 12 500). Introduction of a methyl group at **18**'s NH (**19**) dramatically abated anti-MAO-A activity and selectivity.

The anti-MAO potency displayed by some cyclohexyl derivatives in a preliminary screening (data not shown) and led us to synthesize compounds **27**−**31** as pure enantiomers. The anti-MAO-A activity of **27**−**30** was dependent on the methylcarboxamide rather than the chiral center (compare **28** with **27** and **30** with **29**). On the contrary, as MAO-B inhibitor (*R*)-derivative **29** was 136 times more potent than the corresponding enantiomer (*S*)-**30**, while (*R*)-**27** and (*S*)-**28** were almost equipotent.

Replacing the benzyl of **9** with a propargyl group gave compound **32**. As an MAO-A inhibitor, **32** was as active as **9**. The corresponding *N*-methylcarboxamide **33** was 8 times more potent than **32**. Reduction of **32** to **35** resulted in a significant improvement of the anti-MAO-B activity ($K_i = 0.062$ $\mu$M). The methylated analogue **4** greatly showed improved anti-MAO-A ($K_i = 0.0054$ $\mu$M) and anti-MAO-B ($K_i = 0.02$ $\mu$M) activity. However, this compound was poorly selective.

**Molecular Modeling.** We carried out docking experiments and molecular dynamics (MD) simulations of compounds **7** and

**Table 1.** Structures and Monoamine Oxidase Inhibitory Activities of Derivatives **4** and **7**−**36**[a]

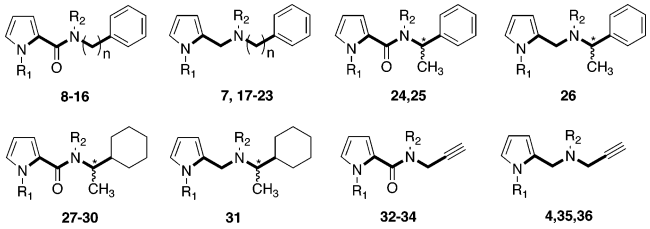


| compd | $R_1$ | $R_2$ | n | * | $K_i$ ($\mu$M) MAO-A | $K_i$ ($\mu$M) MAO-B | SI[b] |
|---|---|---|---|---|---|---|---|
| 8 | H | H | 0 | | 0.4 | >100 | >250.0 |
| **9**[c] | H | H | 1 | | 0.25 | 150 | 600.0 |
| **10**[c] | H | $CH_3$ | 1 | | 0.6 | 150 | 250.0 |
| 11 | H | H | 2 | | 0.42 | >100 | >238.1 |
| 12 | H | $CH_3$ | 2 | | 0.007 | 0.12 | 17.1 |
| 13 | H | H | 3 | | 0.70 | 25 | 35.7 |
| 14 | H | $CH_3$ | 3 | | 0.04 | 8.9 | 222.5 |
| 15 | H | H | 4 | | 0.055 | 57 | 1036.4 |
| 16 | H | $CH_3$ | 4 | | 0.09 | 2.5 | 27.7 |
| 17 | H | H | 1 | | 0.35 | 7.2 | 20.5 |
| **7**[c] | H | $CH_3$ | 1 | | 3.5 | 0.02 | 0.0057 |
| 18 | $CH_3$ | H | 1 | | 0.024 | 300 | 12500.0 |
| **19**[c] | $CH_3$ | $CH_3$ | 1 | | 0.15 | 85 | 566.6 |
| 20 | H | H | 2 | | 0.02 | 0.7 | 35.0 |
| 21 | H | $CH_3$ | 2 | | 0.05 | 4.8 | 96.0 |
| 22 | H | $CH_3$ | 3 | | 0.05 | 2.0 | 40.0 |
| 23 | H | $CH_3$ | 4 | | 0.1 | 2.5 | 25.0 |
| 24 | H | H | | R,S | 1.22 | 61.8 | 50.6 |
| 25 | H | $CH_3$ | | R,S | 0.01 | 4.5 | 450.0 |
| 26 | H | $CH_3$ | | R,S | 0.1 | 1.5 | 15.0 |
| 27 | H | H | | R | 0.26 | 3.6 | 13.8 |
| 28 | H | H | | S | 0.33 | 3.5 | 10.6 |
| 29 | H | $CH_3$ | | R | 0.0017 | 0.03 | 17.6 |
| 30 | H | $CH_3$ | | S | 0.02 | 4.1 | 205.0 |
| 31 | H | $CH_3$ | | R | 0.02 | 7.0 | 350.0 |
| 32 | H | H | | | 0.23 | 70 | 304.3 |
| **33**[c] | H | $CH_3$ | | | 0.075 | 50 | 666.6 |
| 34 | $CH_3$ | $CH_3$ | | | 0.83 | >100 | >120.5 |
| 35 | H | H | | | 0.3 | 0.62 | 2.1 |
| **4**[c] | H | $CH_3$ | | | 0.0054 | 0.02 | 3.7 |
| 36 | $CH_3$ | $CH_3$ | | | 0.44 | >100 | >227.3 |
| MCL[d] | | | | | 11.5 | >100 | >87 |
| CLG[e] | | | | | 0.054 | 58 | 1074.1 |
| SLG[f] | | | | | 3.8 | 0.97 | 0.25 |

[a] Data represent mean values for at least three separate experiments each performed in duplicate. Standard errors were within 2%. [b] SI = $K_i$(MAO-B)/$K_i$(MAO-A) ratio. [c] Reference 11. [d] MCL, moclobemide. [e] CLG, clorgyline. [f] SLG, selegiline.

**Chart 2.** Structure−activity Relationships Remarks[a]

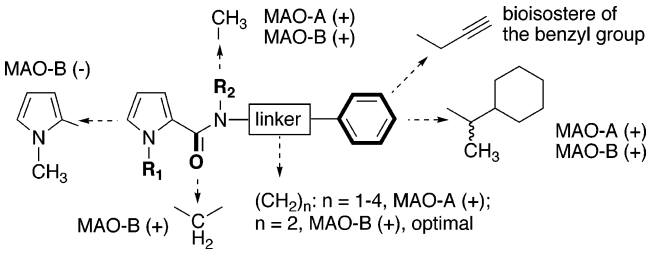


[a] (+) Positive or (−) negative effect of the chemical modifications on the inhibition of the indicated MAO isoform.

**18** using the 3-D X-ray crystal structures of rat MAO-A (PDB code 1O5W)[15] and human MAO-B (PDB code 1GOS).[16] Docking calculations were performed using the automated docking tools AutoDock 3.0.5[17,18] and GOLD 2.2,[19,20] which well reproduced experimentally found binding modes of several ligands.[17,18,21]

In order to take into account the protein flexibility and evaluate the dynamic stability of the predicted ligand/enzyme interactions, all complexes obtained from docking were submitted to MD simulations for 400 ps at 300 K (constant temperature). The dynamic stability of each docked conformation was monitored by computing the root-mean-squared deviations (rmsd) of the ligands, relative to their initial docked orientation. The enzyme−ligand hydrogen bond distances were monitored during the complete MD trajectory.

**Table 2.** Result of 50 Independent Autodock and GOLD Docking Runs for Each Ligand[a]

| ligand | MAO isoform | $N_{tot}$ | $f_{occ}$ | $\Delta G_{bind}$ | GOLD fitness score[b] |
|---|---|---|---|---|---|
| 7 | A | 19 | 20 | −8.75 | 47.6 |
| 7 | B | 8 | 20 | −9.13 | 51.9 |
| 18 | A | 10 | 17 | −8.47 | 52.4 |
| 18 | B | 16 | 13 | −8.45 | 40.2 |

[a] $N_{tot}$ is the total number of clusters; the number of results in the top cluster is given by the frequency of occurrence, $f_{occ}$; $\Delta G_{bind}$(kcal/mol) is the estimated free energy of binding for the top cluster results. [b] Higher scores indicate more favorable binding (kJ/mol).

The use of the crystal structure of rat MAO-A and human MAO-B for docking studies is justified by the following facts: (i) the crystal structures of bovine MAO-A and MAO-B isoforms are unknown; (ii) the rat and bovine sequences of MAO-A are characterized by 85.3% of identity and 95.4% of homology at the binding site, while the human and bovine sequences of MAO-B have 91.3% of identity and 97.1% of homology,[22] and (iii) all active-site residues are largely conserved across the MAO isoforms sequenced so far. Only one mutation is found at the catalytic site of the human and bovine sequence of MAO-B: Ile199 is replaced by Phe199.[23]

AutoDock provided well-clustered docking results for compounds **7** and **18**. The 50 independent docking runs, carried out for each ligand, converged to a small number of different positions ("clusters" of results differing by less than 1.5 Å rmsd). Generally, the top ranking clusters (i.e., those with the most favorable $\Delta G_{bind}$) were also associated with the highest frequency of occurrence, which suggested a good convergence of the search algorithm. The best results in terms of free energy of binding were all located in a similar position into the active site.

Docking studies with GOLD showed that **7** and **18** occupied the same binding locations suggested by AutoDock into the MAO-A and MAO-B. The GOLD run recognized a series of variable conformations of the ligand docked into the binding site, together with an associated scoring function and other measures of the corresponding protein−ligand interaction energy. The GOLD score consisted of hydrogen-bonding, complex energy, and ligand internal-energy terms.

Docking results (the total number of clusters, the number of results in the most populated cluster, the relative estimated free energy of binding, and the GOLD fitness score) are summarized in Table 2.

**Binding Mode of 7 and 18 into MAO-A.** Docking studies of compound **7** into the active site of MAO-A provided well-clustered solutions. The top result ranked with a clearly better score than all other results ($\Delta G_{bind}$ = −8.75 kcal/mol, found 20 times out of 50). Similarly, the top-ranked binding mode obtained for **18** ($\Delta G_{bind}$ = −8.47 kcal/mol, found 17 times out of 50) was located in a comparable position into the active site. Surprisingly, docked conformations of **7** and **18** proposed by GOLD assumed binding poses that strongly resembled the top-ranking ones found by AutoDock, with fitness scores of 47.6 and 52.4 kJ/mol, respectively.

It is worth noting that the scoring functions found by Autodock were not well correlated with the experimental data,

while GOLD found interesting correlations with the experimental data from an energetic point of view. The reason way Autodock gave unsatisfactory results might be a result of some simplifications residing in this software: (A) no explicit water molecules were considered in docking studies; (B) solvation and entropic effects were not taken into account. Accordingly, Binda et al. emphasized the role of structural water molecules into the catalytic region close to the FAD cofactor, also in the presence of noncovalent ligands complexed to the MAO-B isoform.[24] Structural water molecules were neglected in our docking simulations, but we aim to include them in our forthcoming studies.

Visual inspection of the poses of **7** and **18** into the MAO-A binding site revealed that the phenyl rings are placed in the "aromatic cage" and are oriented to establish $\pi-\pi$ stacking interactions with Tyr407 and Tyr444 side chains as well as a T-shaped $\pi-\pi$ interactions with the FAD aromatic ring. Moreover, a hydrogen bond between the protonated amino group of **18** and the carbonyl oxygen of Gln215 side chain is also observed. This H-bond is absent in the **7**/MAO-A complex. The methyl group on the positively charged nitrogen atom of **7** caused an increase of the steric hindrance into the binding cavity, thus preventing from forming a reinforced H bond between the proton on the amino group and the Gln215 residue. In both solutions, the pyrrole ring is embedded in a large hydrophobic pocket formed by Ile180, Phe208, Val210, Ile325, Ile335, Ile337, and Met350.

MD trajectories (data not shown) suggest that MAO-A produces stable complexes with the inhibitors **7** and **18**. Compound **7**, after small amplitude fluctuations in the binding site for 100 ps, rapidly achieves stable interactions with the enzyme key residues throughout the trajectory. The low rmsd (1.45 Å) of compound **18** indicates no significant deviation from the initial docked conformation during the MD simulation for 400 ps. Figure 1 shows the binding mode of **7** (a) and **18** (b) into the MAO-A active site as the average structure calculated on the whole 300 ps of the production step. Visual inspection of the complex models indicates that the higher anti-MAO-A potency of **18** in comparison with **7** ($K_i$ = 0.024 and 3.5 $\mu$M, respectively) may be ascribable to the H-bond between the protonated amino group of **18** and the carbonyl oxygen of Gln215 side chain that is absent in the **7**/MAO-A complex.

**Binding Mode of 7 and 18 into MAO-B.** AutoDock found different binding poses for compounds **7** and **18**, with highly populated clusters (20/50 and 13/50, respectively) and estimated binding free energy of −9.13 and −8.45 kcal/mol, respectively. In contrast, GOLD successfully calculated a single binding pose of **7** and **18** into the MAO-B active site. However, the associated binding orientations strongly resembled the top-ranked ones found by AutoDock, with fitness scores of 51.9 kJ/mol for **7** and 40.2 kJ/mol for **18**.

The phenyl ring of **7** is hosted into the "aromatic cage" framed by Tyr188, Tyr398, Tyr435, and the FAD aromatic ring, where it forms a number of charge-transfer interactions. Unexpectedly, the phenyl ring of **18** is positioned just underneath the enzymatic "aromatic cage" and seems unable to form any charge-transfer interaction with the enzyme. Two H-bonds are also observable for **7** between the protonated aminomethyl group and the phenolic oxygen of Tyr435 and the pyrrole NH and the Gln206 carbonyl oxygen. Compound **18** forms only one H-bond between its protonated amino group and the Gln206 side chain. In both cases, the binding is further stabilized by hydrophobic interactions between the pyrrole ring and a large lipophilic cleft made up by Phe168, Leu171, Ile198, Ile199, and Tyr326 side chains.

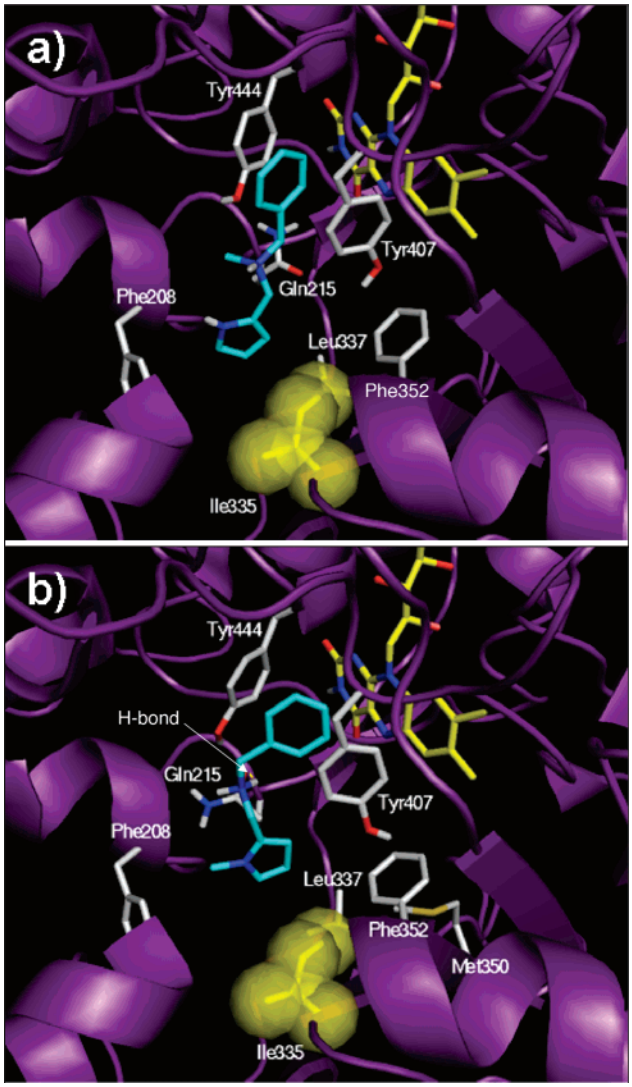


**Figure 1.** Binding modes of compound **7** (a) and **18** (b) into the MAO-A binding cavity. For clarity, only interacting residues are displayed. Ligand (cyan), FAD cofactor (yellow), and interacting key residues (white) are represented as stick models, while the proteins (purple) are represented as ribbons. The van der Waals volume of Ile335 is displayed as a transparent yellow surface.

Analysis of the MD trajectories of compounds **7** and **18** complexed with MAO-B reveals that both ligands adopt a stable binding pose during the simulation time, as confirmed by their low rmsd fluctuations (1.01 Å for **7** and 2.01 Å for **18**). Moreover, the H bonds between **7** and both Tyr435 and Gln206 side chains were also stable throughout the MD simulation, thus explaining the higher anti-MAO-B potency of **7** (**7**, $K_i$ = 0.02 $\mu$M; **18**, 300 $\mu$M). Figure 2 displays the binding mode of **7** (a) and **18** (b) into the MAO-B active site as the average structure calculated on the whole 300 ps of the production step. These results provide a molecular rationale for the MAO-A selectivity of **18**. In fact, the binding pose of **18** into the MAO-B active site seems to be forced by the bulkier Tyr326 residue (displayed as a transparent yellow surface in Figure 2). The Tyr326 residue, which is specific of the MAO-B, is replaced by the smaller Ile residue (Ile335, displayed as a transparent yellow surface in Figure 1) in the MAO-A isoform. This amino acid forces the ligand to adopt a different pose into MAO-B, thus preventing from recurring charge-transfer interactions of the phenyl ring with the "aromatic cage". Ile335 and Tyr326, the major

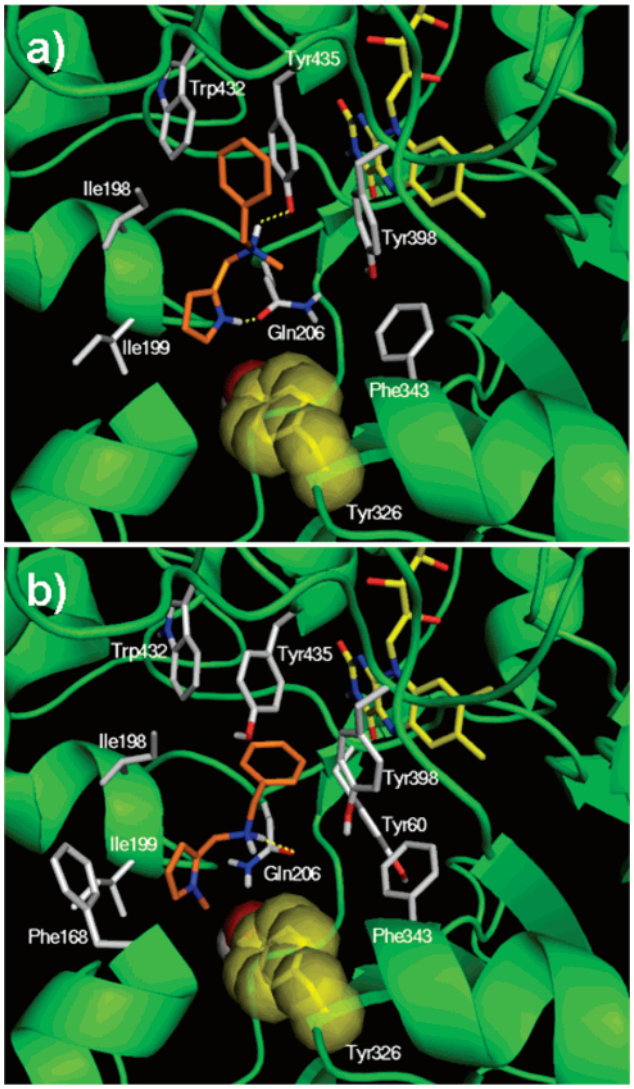


**Figure 2.** Binding modes of compound **7** (a) and **18** (b) into the MAO-B binding cavity. For clarity, only interacting residues are displayed. Ligand (orange), FAD cofactor (yellow), and interacting key residues (white) are represented as stick models, while the proteins (green) are represented as ribbons. The van der Waals volume of Tyr326 is displayed as a transparent yellow surface. H-bonds are shown as dashed yellow lines.

structural differences between the two MAO isoforms,[25] seem to play a significant role in the recognition of these derivatives.

## Conclusions

SAR analysis clarified structural requirements for the good activity and selectivity of this new class of anti-MAO agents. Essential structural features for an active agent have included (Chart 2): (i) a methyl group at the carboxamide function increasead the anti-MAO-A and -B activity; (ii) the length of the linker ($n = 1-4$) had no effect on the anti-MAO-A activity of amides **8**−**16**; (iii) an ethylene linker ($n = 2$, **11** and **12**) yielded compounds with increased anti-MAO-B activity; (iv) reduction of the carbonyl to a methylene resulted in potent MAO-B inhibitors; (v) introduction of a *N*-benzyl,*N*-methyl-amino group (**7**) resulted in compounds with greater anti-MAO-B activity; (vi) a *N*-methyl,*N*-(*R*)-α-(1-cyclohexyl)ethyl-amino group (**29**) increased both MAO-A and MAO-B inhibitory activity, with concomitant loss of selectivity; (vii) the propargyl group was a valid bioisostere of the benzyl for the anti-MAO-A activity of the amides; (viii) introduction of a methyl group at position 1 of the pyrrole resulted in a reduction of anti-MAO-B activity. It is intriguing that the two closely related structures **7** and **18** showed the highest selectivity against the MAO-B (**7,** SI = 0.0057) and the MAO-A (**18**, SI = 12 500).

Docking studies and MD simulations indicated that the high MAO-A inhibitory potency of **18** ($K_i = 0.024$ μM) may be ascribable to the H bond between its protonated amino group and the carbonyl oxygen of Gln215 side-chain. This H-bond is absent in the **7**/MAO-A complex. Conversely, into the MAO-B binding site, **7** forms two H bonds, whereas **18** seems to form only one H bond between the protonated amino group and Gln206 side chain. In the B isoform, the phenyl ring of **7** is hosted into an aromatic cage, where it forms a number of charge-transfer interactions. On the contrary, the phenyl ring of **18** is unable to establish any charge-transfer interaction with the enzyme. This compound seems to be forced by a bulkier Tyr residue, specific of this isoform (into MAO-A this aminoacid is replaced by a smaller Ile residue). We found a molecular rationale for the MAO-A and MAO-B selectivity of this new class of pyrrole inhibitors. These findings increase our confidence in our model and stimulate us to continue our investigations in designing more potent and selective analogues.

## Experimental Section

**Chemistry.** Melting points (mp) were determined on a Büchi 510 apparatus and are uncorrected. Infrared spectra (IR) were run on Perkin-Elmer 1310 and SpectrumOne spectrophotometers. Band position and absorption ranges are given in $cm^{-1}$. Proton nuclear magnetic resonance ($^1H$ NMR) spectra were recorded on Bruker AM-200 (200 MHz) and Bruker Avance 400 MHz FT spectrometers in the indicated solvent. Chemical shifts are expressed in $\delta$ units (ppm) from tetramethylsilane. Column chromatographies were packed with alumina (Merck, 70-230 mesh) and silica gel (Merck, 70-230 mesh). Aluminum oxide thin-layer chromatography (TLC) cards (Fluka, aluminum oxide precoated aluminum cards with fluorescent indicator at 254 nm) and silica gel TLC cards (Fluka, silica gel precoated aluminum cards with fluorescent indicator at 254 nm) were used for TLC. Developed plates were visualized with a Spectroline ENF 260C/F UV apparatus. Organic solutions were dried over anhydrous sodium sulfate. Concentration and evaporation of the solvent after reaction or extraction was carried out on a rotary evaporator (Büchi Rotavapor) operating at reduced pressure. Elemental analyses were found within ±0.4% of the theoretical values.

**General Procedure for the Synthesis of Compounds 8−16, 24, 27, 28, 32, and 33. Example: *N*-Phenyl-1*H*-pyrrole-2-carboxamide (8).** A mixture of 2-trichloroacetyl-1*H*-pyrrole (2.76 g, 0.013 mol), aniline (1.49 g, 1.46 mL, 0.016 mol), and triethylamine (1.62 g, 2.23 mL, 0.016 mol) was heated overnight at 60 °C. The mixture was evaporated in vacuo to give a crude residue which was triturated with *n*-hexane. The solid was filtered, washed with *n*-hexane, and then purified by alumina column chromatography (chloroform as eluent) to afford **8** (1.27 g, 52%) as white crystals, mp 152−155 °C (from benzene). $^1H$ NMR (DMSO-$d_6$): $\delta$ 6.17 (m, 1H), 6.96−7.08 (m, 3H), 7.32 (t, $J = 7.89$ Hz, 2H), 7.74 (d, $J = 7.82$ Hz, 2H), 9.72 (br s, 1H, disappeared on treatment with $D_2O$), 11.62 ppm (br s, 1H disappeared on treatment with $D_2O$). IR: $\nu$ 1635, 2924, 3319 $cm^{-1}$. Anal. Calcd ($C_{11}H_{10}N_2O$ (186.21)) C, H, N.[26]

***N*-Benzyl-1*H*-pyrrole-2-carboxamide (9).** This compound was synthesized as we previously reported.[11]

***N*-Benzyl,*N*-methyl-1*H*-pyrrole-2-carboxamide (10).** This compound was synthesized as we previously reported.[11]

***N*-2-Phenylethyl-1*H*-pyrrole-2-carboxamide (11).** It was synthesized as **8** using 2-phenylethylamine. Yield 87%, mp 125 °C (from toluene). $^1H$ NMR (DMSO-$d_6$): $\delta$ 2.81 (t, $J = 7.45$ Hz, 2H), 3.38−3.49 (m, 2H), 6.04−6.07 (m, 1H), 6.74 (s, 1H), 6.80−6.83 (m, 1H), 7.16−7.37 (m, 5H), 8.09 (br s, disappeared on treatment

with $D_2O$, 1H), 11.42 ppm (br s, disappeared on treatment with $D_2O$, 1H). IR: $\nu$ 1612, 3271, 3381 $cm^{-1}$. Anal. Calcd ($C_{13}H_{14}N_2O$ (214.27)) C, H, N.

***N*-(2-Phenylethyl),*N*-methyl-1*H*-pyrrole-2-carboxamide (12).** It was synthesized as **8** using *N*-methyl-*N*-(*2*-phenylethyl)amine. Yield 39%, oil. $^1H$ NMR ($CDCl_3$): $\delta$ 2.97 (t, $J = 7.43$ Hz, 2H), 3.17 (s, 3H), 3.82 (t, $J = 7.43$ Hz, 2H), 6.25−6.27 (m, 1H), 6.56−6.57 (m, 1H), 6.93 (s, 1H), 7.21−7.25 (m, 3H), 7.29−7.33 (m, 2H), 9.89 ppm (br s, disappeared on treatment with $D_2O$, 1H). IR: $\nu$ 1586, 3240 $cm^{-1}$. Anal. Calcd ($C_{14}H_{16}N_2O$ (228.29)) C, H, N.

***N*-(3-Phenylpropyl)-1*H*-pyrrole-2-carboxamide (13).** It was synthesized as **8** using 3-phenylpropylamine. Yield 57%, mp 80−82 °C (from ethanol). $^1H$ NMR (DMSO-$d_6$): $\delta$ 1.76−1.79 (m, 2H), 2.59 (t, $J = 7.64$ Hz, 2H), 3.18−3.23 (m, 2H), 6.04−6.06 (m, 1H), 6.73 (s, 1H), 6.81 (s, 1H), 7.13−7.21 (m, 5H), 7.97 (br s, disappeared on treatment with $D_2O$, 1H), 11.37 ppm (br s, disappeared on treatment with $D_2O$, 1H); IR: $\nu$ 1590, 3181, 3285 $cm^{-1}$. Anal. Calcd ($C_{14}H_{16}N_2O$ (228.29)) C, H, N.

***N*-(3-Phenylpropyl),*N*-methyl-1*H*-pyrrole-2-carboxamide (14).** It was synthesized as **8** using *N*-methyl-*N*-(3-phenylpropyl)amine. Yield 70%, mp 92 °C (from ethanol). $^1H$ NMR (DMSO-$d_6$): $\delta$ 1.99 (m, 2H), 2.68 (t, $J = 7.74$ Hz, 2H), 3.22 (s, 3H), 3.61 (t, $J = 7.44$ Hz, 2H), 6.23 (s, 1H), 6.51 (s, 1H), 6.92 (s, 1H), 7.19−7.21 (m, 3H), 7.25−7.31 (m, 2H), 9.55 ppm (br s, disappeared on treatment with $D_2O$, 1H). IR: $\nu$ 1587, 3245 $cm^{-1}$. Anal. Calcd ($C_{15}H_{18}N_2O$ (242.32)) C, H, N.

***N*-(4-Phenylbutyl)-1*H*-pyrrole-2-carboxamide (15).** It was synthesized as **8** using 4-phenylbutylamine. Yield 57%, mp 98−100 °C (from ethanol). $^1H$ NMR (DMSO-$d_6$): $\delta$ 1.45−1.51 (q, $J = 7.27$ Hz, 2H), 1.53−1.59 (q, $J = 7.70$ Hz, 2H), 2.58 (t, $J = 7.47$ Hz, 2H), 3.21 (q, $J = 6.53$ Hz, 2H), 6.02−6.04 (m, 1H), 6.70−6.72 (m, 1H), 6.79−6.80 (s, 1H), 7.12−7.18 (m, 3H), 7.22−7.26 (m, 2H), 7.92 (br s, disappeared on treatment with $D_2O$, 1H), 11.35 ppm (br s, disappeared on treatment with $D_2O$, 1H). IR: $\nu$ 1602, 3178, 3279 $cm^{-1}$. Anal. Calcd ($C_{15}H_{18}N_2O$ (242.32)) C, H, N.

***N*-(4-Phenylbutyl),*N*-methyl 1*H*-pyrrole-2-carboxamide (16).** It was synthesized as **8** using *N*-methyl-*N*-(4-phenylbutyl)amine. Yield 40%, mp 75 °C (from ethanol). $^1H$ NMR ($CDCl_3$): $\delta$ 1.66−1.68 (m, 4H), 2.66 (t, $J = 7.11$ Hz, 2H), 3.22 (s, 3H), 3.59 (t, $J = 7.11$ Hz, 2H, 2H), 6.24−6.26 (m, 1H), 6.53 (s, 1H), 6.91 (s, 1H), 7.15−7.20 (m, 3H), 7.25−7.29 (m, 2H), 9.61 ppm (br s, disappeared on treatment with $D_2O$, 1H). IR: $\nu$ 1664, 3225 $cm^{-1}$. Anal. Calcd ($C_{16}H_{20}N_2O$ (256.35)) C, H, N.

**(*R*,*S*)-*N*-(α-Phenylethyl)-1*H*-pyrrole-2-carboxamide (24).** It was synthesized as **8** using (*R*,*S*)-α-phenylethylamine. Yield 35%, mp 144−147 °C (from ethanol). $^1H$ NMR (DMSO-$d_6$): $\delta$ 1.43 (d, $J = 7.00$ Hz, 3H), 5.10−5.14 (m, 1H), 6.06 (d, $J = 8.20$ Hz, 1H), 6.82 (s, 1H), 6.87 (s, 1H), 7.17−7.36 (m, 5H), 8.26 (br s, disappeared on treatment with $D_2O$, 1H), 11.36 ppm (br s, disappeared on treatment with $D_2O$, 1H). IR: $\nu$ 1604, 3285 $cm^{-1}$. Anal. Calcd ($C_{13}H_{14}N_2O$ (214.27)) C, H, N.

**(*R*)-*N*-(α-Cyclohexylethyl)-1*H*-pyrrole-2-carboxamide (27).** It was synthesized as **8** using (*R*)-α-cyclohexylethylamine. Yield 78%, mp 163−166 °C (from ethanol). $^1H$ NMR (DMSO-$d_6$): $\delta$ 0.88−0.92 (m, 2H), 1.03−1.14 (m, 6H), 1.32−1.34 (m, 1H), 1.56−1.71 (m, 5H), 3.76−3.78 (m, 1H), 6.02 (br s, disappeared on treatment with $D_2O$, 1H), 6.77−6.80 (m, 2H), 7.54−7.56 (m, 1H), 11.30 ppm (br s, disappeared on treatment with $D_2O$, 1H). IR: $\nu$ 1602, 3285 $cm^{-1}$. Anal. Calcd ($C_{13}H_{20}N_2O$ (220.31)) C, H, N.

**(*S*)-*N*-(α-Cyclohexylethyl)-1*H*-pyrrole-2-carboxamide (28).** It was synthesized as **8** using (*S*)-α-cyclohexylethylamine. Yield 75%, mp 163−166 °C (from ethanol). $^1H$ NMR (DMSO-$d_6$): $\delta$ 0.88−0.92 (m, 2H), 1.04−1.14 (m, 6H), 1.32−1.35 (m, 1H), 1.56−1.71 (m, 5H), 3.76−3.78 (m, 1H), 6.02 (br s, disappeared on treatment with $D_2O$, 1H), 6.76−6.80 (m, 2H), 7.54−7.56 (m, 1H), 11.30 ppm (br s, disappeared on treatment with $D_2O$, 1H). IR: $\nu$ 1602, 3285 $cm^{-1}$. Anal. Calcd ($C_{13}H_{20}N_2O$ (220.31)) C, H, N.

***N*-Propargyl-1*H*-pyrrole-2-carboxamide (32).** It was synthesized as **8** using propargylamine. Yield 82%, mp 110−112 °C (from ethanol). $^1H$ NMR (DMSO-$d_6$): $\delta$ 2.36 (t, $J = 4.99$ Hz, 1H), 4.00−4.02 (m, 2H), 6.01−6.03 (m, 1H), 6.71−6.73 (m, 1H), 6.74−6.76 (m, 1H), 8.00 (br s, disappeared on treatment with $D_2O$, 1H), 11.00 ppm (br s, disappeared on treatment with $D_2O$, 1H). IR: $\nu$ 1622, 3264, 3283, 3360 $cm^{-1}$. Anal. Calcd ($C_8H_8N_2O$ (148.16)) C, H, N.

***N*-Methyl,*N*-propargyl-1*H*-pyrrole-2-carboxamide (33).** This compound was synthesized as we previously reported.[11]

**General Procedure for the Synthesis of Compounds 25, 29, and 30. Example: (*R*,*S*)-*N*-methyl,*N*-(α-phenylethyl)-1*H*-pyrrole-2-carboxamide (25).** BOP reagent (3.32 g, 0.0075 mol) was added to a solution of pyrrole-2-carboxylic acid (0.83 g, 0.0075 mol), (*R*,*S*)-*N*-methyl-α-phenylethylamine (2.03 g, 0.015 mol), and triethylamine (2.28 g, 3.17 mL, 0.0225 mol) in anhydrous DMF (5 mL). The reaction mixture was stirred at room temperature overnight. Water was added while stirring, and the mixture was extracted with ethyl acetate. The organic layer was separated, washed with brine, and dried. The solvent was evaporated to afford a residue which was purified by silica gel column chromatography (ethyl acetate as eluent). $^1H$ NMR ($CDCl_3$): $\delta$ 1.61 (d, $J = 6.95$ Hz, 3H), 2.94 (s, 3H), 6.19 (m, 1H), 6.24−6.25 (m, 1H), 6.57 (s, 1H), 6.95 (s, 1H), 7.26−7.38 (m, 5H), 9.94 ppm (br s, disappeared on treatment with $D_2O$, 1H). IR: $\nu$ 1583, 3251 $cm^{-1}$. Anal. Calcd ($C_{14}H_{16}N_2O$ (228.29)) C, H, N.

**(*R*)-*N*-(α-Cyclohexylethyl),*N*-methyl-1*H*-pyrrole-2-carboxamide (29).** It was prepared as **25** using (*R*)-*N*-methyl-*N*-(α-cyclohexylethyl)amine. Yield 61%, oil. $^1H$ NMR ($CDCl_3$): $\delta$ 0.8−1.06 (m, 2H), 1.12−1.25 (m, 6H), 1.40−1.42 (m, 1H), 1.58−1.63 (m, 3H), 1.75−1.81 (m, 2H), 3.12 (s, 3H), 4.53−4.57 (m, 1H), 6.21 (s, 1H), 6.59 (s, 1H), 6.92 (s, 1H), 9.77 ppm (br s, disappeared on treatment with $D_2O$, 1H). IR: $\nu$ 1578, 3252 $cm^{-1}$. Anal. Calcd ($C_{14}H_{22}N_2O$ (234.34)) C, H, N.

**(*S*)-*N*-(α-Cyclohexylethyl),*N*-methyl-1*H*-pyrrole-2-carboxamide (30).** It was synthesized as **25** using (*S*)-*N*-methyl-*N*-(α-cyclohexylethyl)amine. Yield 85%, oil. $^1H$ NMR ($CDCl_3$): $\delta$ 0.8−1.06 (m, 2H), 1.12−1.25 (m, 6H), 1.40−1.42 (m, 1H), 1.58−1.63 (m, 3H), 1.75−1.81 (m, 2H), 3.12 (s, 3H), 4.53−4.57 (m, 1H), 6.21 (m, 1H), 6.59 (m, 1H), 6.92 (m, 1H), 9.77 ppm (br s, disappeared on treatment with $D_2O$, 1H). IR: $\nu$ 1578, 3252 $cm^{-1}$. Anal. Calcd ($C_{14}H_{22}N_2O$ (234.34)) C, H, N.

***N*-Propargyl,*N*-methyl-1-methyl-1*H*-pyrrole-2-carboxamide (34).** Iodomethane (0.85 g, 0.37 mL, 0.006 mol) was added to an ice-cooled mixture of **33** (0.32 g, 0.002 mol), tetrabutylammonium hydrogen sulfate (0.68 g, 0.002 mol), dichlorometane (10 mL), and 50% NaOH solution (7 mL). The reaction was stirred at room temperature overnight. Water was added while stirring and the mixture extracted with dichlorometane. The organic layer was separated, washed with brine, and dried. The solvent was evaporated to afford a residue which was purified by silica gel column chromatography (chloroform as eluent). Yield 57%, oil. $^1H$ NMR DMSO-$d_6$: $\delta$ 2.36 (t, $J = 4.87$ Hz, 1H), 3.07 (s, 3H), 3.68 (s, 3H), 4.28 (d, $J = 4.87$ Hz, 2H), 6.04−6.07 (m, 1H), 6.48−6.50 (m, 1H), 6.91−6.93 ppm (m, 1H). IR: $\nu$1622, 2116, 3108, 3285, 3487 cm.[1] Anal. Calcd ($C_{10}H_{12}N_2O$ (176.22)) C, H, N.

**General Procedure for the Synthesis of Compounds 4, 7, 19, 21, 22, 23, 26, 31, and 36. Example: *N*-Methyl,*N*-(2-phenylethyl),*N*-(pyrrol-2-ylmethyl)amine (21).** Formaldehyde (37% water solution, 0.41 mL, 0.016 mol) and *N*-methyl-2-phenylethylamine (2.16 g, 0.016 mol) were added to an ice-cooled solution of pyrrole (1.07 g, 0.016 mol) in acetonitrile (42 mL). The reaction was stirred for 30 min at room temperature. After quenching on crushed ice, the mixture was made basic with 50% NaOH and extracted with ethyl acetate. The organic layer was separated, washed with brine, and dried. The solvent was evaporated to give a residue that was purified by alumina column chromatography (chloroform a eluent). Yield 7%, oil. $^1H$ NMR ($CDCl_3$): $\delta$ 2.31 (s, 3H), 2.64 (t, $J = 7.52$ Hz, 2H), 2.79 (t, $J = 7.52$ Hz, 2H), 3.55 (s, 2H), 6.00 (s, 1H), 6.09−6.11 (m, 1H), 6.63−6.64 (m, 1H), 7.17−7.32 (m, 5H), 8.21 ppm (br s, disappeared on treatment with $D_2O$, 1H). IR: $\nu$ 3428 $cm^{-1}$. Anal. Calcd ($C_{14}H_{18}N_2$ (214.31)) C, H, N.

***N*-Methyl,*N*-(propargyl),*N*-(pyrrol-2-ylmethyl)amine (4).** This compound was synthesized as we previously reported.[11]

***N*-Methyl,*N*-(benzyl),*N*-(pyrrol-2-ylmethyl)amine (7).** This compound was synthesized as we previously reported.[11]

***N*-Methyl,*N*-(benzy),*N*-(1-methylpyrrol-2-ylmethyl)amine (19).** This compound was synthesized as we previously reported.[11]

***N*-Methyl,*N*-(3-phenylpropyl),*N*-(pyrrol-2-ylmethyl)amine (22).** It was synthesized as **21** using *N*-methyl,*N*-(3-phenylpropyl)amine. Yield 9%, oil. $^1$H NMR ($CDCl_3$): $\delta$ 1.78−1.86 (q, $J$ = 7.55 Hz, 2H), 2.18 (s, 3H), 2.40 (t, $J$ = 7.36 Hz, 2H), 2.62 (t, $J$ = 7.71 Hz, 2H), 3.49 (s, 2H), 6.00 (s, 1H), 6.11−6.13 (m, 1H), 6.71−6.73 (m, 1H), 7.17−7.21 (m, 3H), 7.25−7.30 (m, 2H), 8.55 ppm (br s, disappeared on treatment with $D_2O$, 1H). IR: $\nu$ 3379 cm$^{-1}$. Anal. Calcd ($C_{15}H_{20}N_2$ (228.34)) C, H, N.

***N*-Methyl,*N*-(3-phenylbutyl),*N*-(pyrrol-2-ylmethyl)amine (23).** It was synthesized as **21** using *N*-methyl,*N*-(3-phenylbutyl)amine. Yield 6%, oil. $^1$H NMR ($CDCl_3$): $\delta$ 1.52−1.60 (m, 4H), 2.21 (s, 3H), 2.42 (t, $J$ = 7.35 Hz, 2H), 2.59 (t, $J$ = 7.29 Hz, 2H), 3.54 (s, 2H), 6.02 (s, 1H), 6.10−6.11 (m, 1H), 6.73−6.74 (m, 1H), 7.13−7.19 (m, 3H), 7.25−7.28 (m, 2H), 8.98 ppm (br s, disappeared on treatment with $D_2O$, 1H). IR: $\nu$ 3339 cm$^{-1}$. Anal. Calcd ($C_{16}H_{22}N_2$ (242.37)) C, H, N.

**(*R*,*S*)-*N*-Methyl,*N*-(α-phenylethyl),*N*-(pyrrol-2-ylmethyl)-amine (26).** It was synthesized as **21** using (*R*,*S*)-*N*-methyl,*N*-(α-phenylethyl)amine. Yield 14%, oil. $^1$H NMR ($CDCl_3$): $\delta$ 1.40 (d, $J$ = 6.80 Hz, 3H), 2.16 (s, 3H), 3.40 (d, $J$ = 13.84 Hz, 1H), 3.55 (d, $J$ = 13.84 Hz, 1H), 3.63 (q, $J$ = 6.79 Hz, 1H), 5.99 (s, 1H), 6.11−6.13 (m, 1H), 6.72−8.74 (m, 1H), 7.24−7.37 (m, 5H), 8.23 ppm (br s, disappeared on treatment with $D_2O$, 1H). IR: $\nu$ 3436 cm$^{-1}$. Anal. Calcd ($C_{14}H_{18}N_2$ (214.31)) C, H, N.

**(*R*)-*N*-(α-Cyclohexylethyl)-*N*-methyl,*N*-(pyrrol-2-ylmethyl)-amine (31).** It was synthesized as **21** using (*R*)-*N*-(α-cyclohexylethyl)-*N*-methylamine. Yield 15%, oil. $^1$H NMR ($CDCl_3$): $\delta$ 0.85−0.93 (m, 6H), 1.16−1.28 (m, 7H), 2.10 (s, 3H), 2.29−2.31 (m, 1H), 2.60−2.63 (m, 1H), 3.49 (d, $J$ = 12 Hz, 1H), 3.62 (d, $J$ = 11.5 Hz, 1H), 5.97−5.99 (m, 1H), 6.12−6.14 (m, 1H), 6.73−6.74 (m, 1H), 8.47 ppm (br s, disappeared on treatment with $D_2O$, 1H). Anal. Calcd ($C_{14}H_{24}N_2$ (220.36)) C, H, N.

***N*-Methyl,*N*-(propargyl),*N*-(1-methylpyrrol-2-ylmethyl)-amine (36).** It was synthesized as **21** using 1-methyl-1*H*-pyrrole and *N*-methylpropargylamine. Yield 5%, mp 148−155 °C (from benzene). $^1$H NMR ($CDCl_3$): $\delta$ 2.25 (t, $J$ = 4.7 Hz, 1H), 2.27 (d, $J$ = 4.7 Hz, 2H), 2.29 (s, 3H), 3.49 (s, 2H), 3.63 (s, 3H), 6.01−6.04 (m, 2H), 6.57−6.60 ppm (m, 1H). IR: $\nu$ 3094, 2725, 2116 cm$^{-1}$. Anal. Calcd ($C_{10}H_{14}N_2$ (162.23)) C, H, N.

***N*-(Benzyl),*N*-(pyrrol-2-ylmethyl)amine (17).** A mixture of pyrrole-2-carboxaldehyde (1.0 g, 0.01 mol) and benzylamine (2.14 g, 2.18 mL, 0.02 mol) was heated at 50 °C for 1 h. After cooling, the reaction mixture was evaporated and the crude product was triturated with *n*-hexane to give *N*-benzyl-*N*-(1*H*-pyrrol-2-ylmethylene)amine as a white solid (1.7 g, 92%).[27] A solution of the latter compound (0.5 g, 0.0027 mol) in THF (4.4 mL) and isopropanol (13.2 mL) was added to a mixture of sodium cyanoborohydride (0.19 g, 0.003 mol) and 1 N HCl in anhydrous diethylether (4 mL) at 0 °C. The reaction was stirred for 10 min at room temperature, then made basic with potassium carbonate saturated solution, and extracted with ethyl acetate. The organic layer was separated, washed with brine, and dried. The solvent was evaporated to give a residue that was purified by silica gel column chromatography (chloroform as eluent). Yield 44%, mp 95−98 °C (toluene/cyclohexane). $^1$H NMR (DMSO-$d_6$): $\delta$ 3.80 (s, 2H), 3.81 (s, 2H), 4.37 (br s, disappeared on treatment with $D_2O$, 1H), 5.94−6.00 (m, 2H), 6.71 (s, 1H), 7.26−7.42 (m, 5H), 10.81 ppm (br s, disappeared on treatment with $D_2O$, 1H). IR: $\nu$ 3375, 3297 cm$^{-1}$. Anal. Calcd ($C_{12}H_{14}N_2$ (186.26)) C, H, N.

***N*-(2-Phenylethyl),*N*-(pyrrol-2-ylmethyl)amine (20).** It was synthesized as **17** using 2-phenylethylamine. The intermediate reaction gave *N*-(2-phenylethyl)-*N*-(1*H*-pyrrol-2-ylmethylene)amine, yield 79%, mp 98−101 °C (cyclohexane). $^1$H NMR (DMSO-$d_6$): $\delta$ 2.70−2.87 (m, 4H), 2.77 (s, 2H), 3.99 (br s, disappeared on treatment with $D_2O$, 1H), 5.93−5.95 (m, 2H), 6.65−6.69 (m, 1H), 7.06−7.33 (m, 5H), 10.71 ppm (br s, disappeared on treatment with $D_2O$, 1H). IR: $\nu$ 2425, 3314 cm$^{-1}$. Sodium cyanoborohydride reduction afforded **20**, yield 27%, oil. $^1$H NMR (DMSO-$d_6$): $\delta$ 2.80 (m, 4H), 3.78 (s, 2H), 3.99 (br s, disappeared with treatment with $D_2O$, 1H), 5.93−5.95 (m, 2H), 6.66−6.69 (m, 1H), 7.18−7.22 (m, 3H), 77.25−7.33 (m, 2H), 10.71 ppm (br s, disappeared on treatment with $D_2O$, 1H); IR: $\nu$ 3314 cm$^{-1}$. Anal. Calcd ($C_{13}H_{16}N_2$ (200.28)) C, H, N.

***N*-(Propargyl),*N*-(pyrrol-2-ylmethyl)amine (35).** To a solution of pyrrole-2-carboxaldehyde (1.0 g, 0.01 mol) in THF (62.5 mL) was added propargylamine (2.75 g, 3.43 mL, 0.05 mol). The reaction mixture was stirred at room temperature for 24 h over molecular sieves 3 Å and filtered. Collected solvent was evaporated to give *N*-(propargyl),*N*-(pyrrol-2-ylmethylene)amine (1.1 g, 85%) as a yellow oil, which was used without further purification. Sodiun borohydride (0.42 g, 0.0011 mol) was added to an ice-cooled solution of the latter amine (1.32 g, 0.01 mol) in methanol (73 mL). The reaction was stirred at room temperature for 45 min. The solvent was distilled, water was added, and the mixture was extracted with ethyl acetate. The organic layer was separated, washed with brine, and dried. The solvent was evaporated to afford a brownish oil that solidified on standing. The crude product was purified by alumina column chromatography (ethyl acetate as eluent) to afford **20**, yield 52%, mp 50 °C (from cyclohexane). $^1$H NMR (DMSO-$d_6$): $\delta$ 3.06 (t, $J$ = 4.7 Hz, 1H), 3.24 (d, $J$ = 4.81 Hz, 2H), 3.65 (s, 2H), 4.12 (br s, disappeared with treatment with $D_2O$, 1H), 5.86−5.90 (m, 2H), 6.60−6.61 (m, 1H), 10.56 ppm (br s, disappeared on treatment with $D_2O$, 1H); IR: $\nu$ 2117, 3176, 3250, 3272 cm$^{-1}$. Anal. Calcd ($C_8H_{10}N_2$ (134.18)) C, H, N.

***N*-(2-Benzyl),*N*-(1-methylpyrrol-2-ylmethyl)amine (18).** A solution of 6 N HCl in MeOH (1:1) (15 mL) and benzylamine (0.98 g, 0.0016 mol) was added to a mixture of 1-methylpyrrole-2-carboxaldehyde (1.0 g, 0.0092 mol), THF (114 mL), and methanol (114 mL). After stirring for 30 min at 0 °C, sodium cyanoborohydride (0.678 g, 0.0108 mol) was added, then the reaction mixture was stirred overnight while the reaction temperature was warmed to room temperature. The solvent was evaporated, water was added, and the mixture was extracted with ethyl acetate. The organic layer was separated, washed with brine, and dried. The solvent was evaporated to afford a brownish oil that solidified on standing. The crude product was purified by alumina gel column chromatography (chloroform as eluent). Yield 62%, mp 215−223 °C (from cyclohexane). $^1$H NMR ($CDCl_3$): $\delta$ 3.63 (s, 3H), 3.73 (s, 2H), 3.82 (s, 2H), 6.03−6.06 (m, 2H), 6.58 (t, $J$ = 4.21 Hz, 1H), 7.25−7.36 (m, 5H), 8.22 ppm (br s, disappeared on treatment with $D_2O$, 1H). IR: $\nu$ 3318, cm$^{-1}$. Anal. Calcd ($C_{13}H_{16}N_2$ (200.28)) C, H, N.

**Biology. Mitochondria Preparation.** Mitochondria were prepared according to Basford.[13] The following reagents were used. Reagents: medium A contained 0.4 M sucrose, 0.001 EDTA, 0.02% PES or heparin and pH value was adjusted to 6.8−7.0 by addition of KOH; medium F made was made up of the medium A to which Ficoll was added to a final concentration of 8%. Calf or beef brains were removed from the animals within 5−10 min after their death. The brains were immediately placed in cold medium A and then stored on ice, to be transported to the laboratory. In a cold room, at 5 °C, the cerebral hemispheres were removed from the brains and the meninges were taken up with forceps. The gray matter was scraped from the cortices using a dull spatula. Two brains yield corresponded to about 100 g of wet tissue, which was homogenized in 2 mL Medium A (2 mL/g of wet tissue). The homogenate was kept at pH 7.0 by adding of some drops of Tris buffer 2 M and 1 mg of $\epsilon$-aminocaproic acid/g of tissue. Then the mixture was stirred at 0−4 °C for 15 min. The suspension was diluted with medium A (20 mL/g of the original tissue) and centrifuged twice, first at 184 g for 20 min and then without transferring of the supernatant at 1153 g for others for 20 min. The residue $R_1$ was discarded, while the supernatant $S_1$ was centrifuged at 12 000 g for 15 min, to yield a crude mitochondria pellet $R_2$, the supernatant $S_2$ was discarded. The fraction $R_2$ was dissolved in medium F (6 mL/g of original tissue), gently homogenized, and centrifuged at 12 000 g for 30 min. The resulting mitochondria fraction $R_3$ was washed using 4 mL of medium A/g of original tissue and again centrifuged at 12 000 g for 15 min to yield the final mitochondria fraction $R_4$, which was homogenized in potassium phosphate buffer pH 7.4,

0.25 M. The yield of mitochondria protein obtained was between 100 and 140 mg per 50 g wet weight of the original tissue.

**Activity Assay.** Mono amine oxidase activity was determined using kinuramine as a substrate, at four different final concentrations ranging from 5 $\mu$M to 0.1 mM, by a sensitive fluorometric assay according to Matsumoto et al.[14] In all assays the incubation mixtures contained: potassium phosphate buffer pH 7.4, mitochondria (6 mg/mL), drug solutions in DMSO, added to the reaction mixture at a final concentration ranging from 0 to $10^{-3}$ $\mu$M. Solutions were preincubated for 30 min before adding the substrate and then incubated for others 30 min. The inhibitory activities of both MAO-A and MAO-B separately were determined after incubation of the mitochondrial fractions for 30 min at 38 °C, in the presence of the specific inhibitor (L-deprenyl 1 $\mu$M to estimate the MAO A activity or clorgyline 1 $\mu$M to assay the isoform B). It was taken into account that MAO-A is irreversibly inhibited by low concentration of clorgyline but is unaffected by low concentration of L-deprenyl, utilized contrary in the form MAO-B. The addition of percloric acid ended the reaction. Then the samples were centrifuged at 10 000 g for 5 min, and the supernatant was added to 2.7 mL of 1 N NaOH. Fluorometric measurements were recorded at $\lambda_{exc}$ 317 nm and $\lambda_{em}$ 393 nm, using a Perkin-Elmer LS 50B spectrofluorometer. The protein concentration was determined according to Goa.[28] Dixon plot were used to estimate the inhibition constant ($K_i$) of the inhibitors. Data are the means of three or more experiments each performed in duplicate.

**Computational Chemistry.** Molecular modeling and graphics manipulations were performed using the SYBYL software package (Sybyl Molecular Modeling System, version 7.0, Tripos Inc., St. Louis, MO), running it on a Silicon Graphics Tezro R16000 workstation. Model building of compounds **7** and **18** was accomplished with the TRIPOS force field[29] available within SYBYL. Point charges for the inhibitors were calculated using the Gasteiger-Marsili method.[30] Energy minimizations of the **7**/MAO-A, **7**/MAO-B, **18**/MAO-A, and **18**/MAO-B complexes were realized by employing the INSIGHT II/DISCOVER software packages (Insight II Molecular Modeling Package and Discover 2.2000 Simulation Package, Accelrys Inc., San Diego, CA), selecting the CVFF force field.[31]

**Docking Simulations.** Docking was performed using AutoDock 3.0.5[17,18] and GOLD 2.2[19,20] software packages. AutoDock combines a rapid energy evaluation through precalculated grids of affinity potentials with a variety of search algorithms to find suitable binding positions for a ligand on a given protein. While the protein is required to be rigid, the Autodock allows torsional flexibility in the ligand. GOLD is an automated ligand-docking program that uses a genetic algorithm to explore the full range of ligand conformational flexibility. Moreover, it permits some protein conformational freedom in the sense that torsion angles of serine, threonine, and tyrosine hydroxyl groups as well as lysine amine groups are optimized by the search algorithm during the posing. These groups are allowed to rotate freely to favor intramolecular (with other residues of the protein) and intermolecular (with the ligand trial solution) H-bond formation. GOLD requires a user-defined binding site. It searches for a cavity within the defined area, and considers all the solvent-accessible atoms in that area as active-site atoms. On the basis of the GOLD score, for each molecule a bound conformation with high score was considered as the best bound conformation. The score function that was implemented in GOLD consisted basically of H-bonding, complex energy, and ligand internal energy terms. A population of possible docked orientations of the ligand is set up at random. Each member of the population is encoded as a "chromosome", which contains information about the mapping of ligand H-bond atoms onto (complementary) protein H-bond atoms, mapping of hydrophobic points of the ligand onto protein hydrophobic points, and the conformation around flexible ligand bonds and protein OH groups. A number of parameters control the precise operation of the genetic algorithm.

**Ligand Setup.** The structures of the ligands **7** and **18** were constructed using standard bond lengths and bond angles of the SYBYL fragment library. The ligands were modeled in their protonated form. Geometry optimizations were carried out with the SYBYL/MAXIMIN2 minimizer by applying the BFGS (Broyden, Fletcher, Goldfarb, and Shannon) algorithm[32] and setting a rms gradient of the forces acting on each atom of 0.001 kcal mol$^{-1}$ Å$^{-1}$ as the convergence criterion. Partial atomic charges were assigned by using the Gasteiger-Marsili formalism.

**Protein Setup.** The crystal structures of MAO-A (entry code: 1O5W)[15] and of MAO-B (entry code: 1GOS)[16] recovered from Brookhaven Protein Database[33] were used. The structures were set up for docking as follows: polar hydrogens were added by using the BIOPOLYMERS module within the SYBYL program (residues Arg, Lys, Glu, and Asp were considered ionized, while all His were considered to be neutral by default), Kollman united atom partial charges were assigned, and all waters were removed.

Original PDB structures were subjected to a preliminary constrained energy minimization of those residues out of a radius of 15 Å from the N5 of the isoalloxazine ring in order to restore the natural planarity of the isoalloxazine FAD ring and relax the active site aminoacids. In the resulting energy minimized structures, the covalent ligands (pargyline for 1GOS and clorogyline for 1O5W) were removed and used as starting models for docking simulations.

**AutoDock Docking.** Docking of compounds **7** and **18** to both MAO-A and MAO-B was carried out using the empirical freeenergy function and the Lamarckian genetic algorithm, applying a standard protocol with an initial population of 50 randomly placed individuals, a maximum number of $1.5 \times 10^6$ energy evaluations, a mutation rate of 0.02, a crossover rate of 0.80, and an elitism value of 1. Proportional selection was used, where the average of the worst energy was calculated over a window of the previous 10 generations. For the local search, the so-called pseudo Solis and Wets algorithm was applied by using a maximum of 300 iterations. The probability of performing local search on an individual in the population was 0.06, and the maximum number of consecutive successes or failures before doubling or halving the local search step size was 4.

Fifty independent docking runs were carried out for each ligand. Results differing by less than 1 Å in positional rmsd were clustered together and represented by the result with the most favorable free energy of binding ($\Delta G_{bind}$). Finally, the compounds were set up for docking with the help of AutoTors, the main purpose of which is to define the torsional degrees of freedom to be considered during the docking process. All torsion angles for each compound were considered flexible. Solvation parameters were added to the final protein file by using the ADDSOL utility of AutoDock. The grid maps representing the proteins in the actual docking process were calculated with AutoGrid. The grids (one for each atom type in the ligand plus one for electrostatic interactions) were chosen to be sufficiently large to include not only the active site but also significant portions of the surrounding surface. The dimensions of the grids were thus 60 Å × 60 Å × 60 Å, with a spacing of 0.375 Å between the grid points. The grid center was centered on the FAD N5 atom using the original PDB models without their covalent ligands.

**GOLD Docking.** An active site of radius 15 Å was defined considering the phenolic oxygen atom of Tyr435 and Tyr444 as the center of the MAO-B and MAO-A, respectively. Fifty independent docking runs were performed for each docking experiment. All docking runs were carried out using standard default settings with a population size of 100, a maximum number of 100 000 operations, and a mutation and crossover rate of 95. The best generated 10 solutions of each ligand were ranked according to their fitness scores calculated by the GOLD Chem-Score function.

**Molecular Dynamics Simulations.** Refinement of the inhibitor/enzyme complexes was achieved by energy minimization with the CVFF force field, permitting only the ligand and the side chain atoms of the protein within a radius of 10 Å around the ligand to relax. Calculations were performed by 3000 steps of steepest descents and 2000 steps of conjugate gradients (down to a maximal atomic rmsd of 10.0 and 0.01 kcal/Å, respectively). The geometry-optimized complexes were then used as the starting point for

subsequent 400 ps MD simulation, during which the protein backbone atoms were constrained as done in the previous step. A distance-dependent dielectric of 40 was applied. The cutoff radius for nonbonded interactions was 12 Å, with a secondary cutoff radius of 15 Å. The molecular system was allowed to equilibrate to 300 K for 100 ps and then kept at this temperature throughout the 300 ps of production run, with a step length of 1 fs. Coordinates were saved every 1 ps and used to calculate the averaged structures from the simulations. The averaged structures over the last 300 ps of the simulations were energy minimized as previously described and stored as the final conformation of the ligand−enzyme complexes.

**Acknowledgment.** This work was partially supported by the Italian MIUR (Ministero dell'Istruzione, dell'Università e della Ricerca) and by funds MIUR-PRIN 2005 (Cofin) (EA).

**Supporting Information Available:** Elemental analyses of new derivatives **8**, **11**−**18**, **20**−**32**, and **34**−**36**. This material is available free of charge via Internet at http://pubs.acs.org.

## References

(1) Mondovì, B. *Structure and function of amine oxidases*; CRC Press, Boca Raton, FL, 1985.
(2) Bach, A. W. J.; Lan, N. C.; Johnson, D. L.; Abell, C. W.; Bembenek, M. E.; Kwan, S. W.; Seeburg, P. H.; Shih, J. C. cDNA cloning of human liver monoamine oxidase A and B: molecular basis of differences in enzymatic properties. *Proc. Natl. Acad. Sci. U.S.A.* **1988**, *85*, 4934−4938.
(3) Abell, C. W.; Kwan, S.-W. Molecular characterization of monoamine oxidases A and B. *Prog. Nucl. Acid Res. Mol. Biol.* **2001**, *65*, 129−156.
(4) Tipton, K. F.; Boyce, S.; O'Sullivan, J.; Davey, G. P.; Healey, J. Monoamine oxidases: certainties and uncertainties. *Curr. Med. Chem.* **2004**, *11*, 1965−1982.
(5) Andrews, J. M.; Nemeroff, C. B. Contemporary management of depression. *Am. J. Med. Chem.* **1994**, *97*, 24S−32S.
(6) Cesura, A. M.; Pletscher, A. The new generation of monoamine oxidase inhibitors. *Prog. Drug Res.* **2002**, *38*, 171−298.
(7) Drukarch, B.; van Muiswinkel, F. L. Drug Treatment of Parkinson's Disease. *Biochem. Pharm.* **2000**, *59*, 1023−1031.
(8) (a) Checkoway, H.; Franklin, G. M.; Costa-Mallen, P.; Smith-Weller, T.; Dilley, J.; Swansons, P. D.; Costa, L. G. A genetic polymorphism of MAO-B modifies the association of cigarette smoking and Parkinson's disease. *Neurology* **1998**, *50*, 1458−1461. (b) Fowler, J. S.; Logan, J.; Wang, G.-J.; Volkow, N. D. Monoamine oxidase and cigarette smoking. *Neurotoxicology* **2003**, *24*, 75−82.
(9) Perez, V.; Unzeta, M. PF9601N, [*N*-(2-propyl)-2-(5-benzyloxy indolyl)methylamine], a new MAO-B inhibitor, attenuates MPTP-induced depletion of striatal dopamine levels in C57/BL6 mice. *Neuchem. Int.* **2003**, *42*, 221−229.
(10) Petzer, J. P.; Steyn, S.; Castagnoli, K. P.; Chen, J.-F.; Schwarzschild, M. A.; Van der Schyf, C. J.; Castagnoli, N. Inhibition of monoamine oxidase B by selective adenosine $A_{2A}$ receptor antagonits. *Bioorg. Med. Chem.* **2003**, *11*, 1299−1310.
(11) Silvestri, R.; La Regina, G.; De Martino, G.; Artico, M.; Befani, O.; Palumbo, M.; Agostinelli, E.; Turini, M. Simple, Potent and Selective Pyrrole Inhibitors of Monoamine Oxidase Type A and Type B. *J. Med. Chem.* **2003**, *46*, 917−920.
(12) Bailey, D. M.; Johnson, R. E.; Albertson, N. F. Ethyl pyrrole-2-carboxylate. *Org. Synth.* **1971**, *51*, 100−102.
(13) Basford, R. E. Preparation and properties of brain mitochondria. *Methods Enzymol.* **1967**, *10*, 96−101.
(14) Matsumoto, T.; Suzuki, O.; Furuta, T.; Asai, M.; Kurokawa, Y.; Rimura, Y.; Katsumata, Y.; Takahashi, I. A sensitive fluorometric assay for serum monoamine oxidase with kynuramine as substrate. *Clin. Biochem.* **1985**, *18*, 126−129.
(15) Ma, J.; Yoshimura, M.; Yamashita, E.; Nakagawa, A.; Ito, A.; Tsukihara, T. Structure of Rat Monoamine Oxidase A and Its Specific Recognitions for Substrates and Inhibitors. *J. Mol. Biol.* **2004**, *338*, 103−114.
(16) Binda, C.; Newton-Vinson, P.; Hubàlek, F.; Edmondson, D. E.; Mattevi, A. Structure of Human Monoamine Oxidase B, a Drug Target for the Treatment of Neurological Disorders. *Nat. Struct. Biol.* **2002**, *9*, 22−26.
(17) Morris, G. M.; Goodsell, D. S.; Halliday, R. S.; Huey, R.; Hart, W. E.; Belew, R. K.; Olson, A. J. Automated Docking Using a Lamarckian Genetic Algorithm and an Empirical Binding Free Energy Function. *J. Comput. Chem.* **1998**, *19*, 1639−1662.
(18) Goodsell, D. S.; Morris, G. M.; Olson, A. J. Automated docking of flexible ligands: applications of AutoDock. *J. Mol. Recognit.* **1996**, *9*, 1−5.
(19) GOLD 2.2; CCDC Software Limited: Cambridge, UK, 2004.
(20) Jones, G.; Willett, P.; Glen, R. C.; Leach, A. R.; Taylor, R. Development and validation of a genetic algorithm for flexible docking. *J. Mol. Biol.* **1997**, *267*, 727−748.
(21) Wang, R.; Lu, Y.; Wang, S. Comparative evaluation of 11 scoring functions for molecular docking. *J. Med. Chem.* **2003**, *46*, 2287−2303.
(22) Database searching (SWISS-PROT), sequence alignment, and analysis of rat, bovine and human MAO sequences were carried out using FASTA (Pearson, W. R. *Proc. Natl. Acad. Sci. U.S.A.* **1988**, *85*, 2444−2448.) and BLAST programs (Wang, S.; Pak, Y. J. *Phys. Chem. B.* **2000**, *104*, 354−359.).
(23) Crystallographic analysis of human MAO-B in complex with several inhibitors (PDB codes: 1S2Q, 1S2Y, 1S3E, and 1S3B) revealed the presence of two cavities inside the protein: the "substrate" cavity (in front of the flavin ring) and the "entrance" cavity (a channel towards the catalytic site). The side chain of Ile199 is as a key structural element that opens and closes the connection between the two cavities. In the closed-conformation, Ile199 physically separates the two cavities. In the presence of bulky ligands this residue adopts an open conformation that allows the ligand to reach the susbtrate cavity. We used the crystal structure of the human MAO-B/pargyline complex, which is characterized by an Ile199 open conformation. Ile199 is conserved in all the known MAO-B sequences, with the only exception of bovine MAO-B, where it is replaced with Phe. Edmondson et al. (Hubàlek, F.; Binda, C.; Khalil, A.; Li, M.; Mattevi, A.; Castagnoli, N.; Edmondson, D. E. Demonstration of isoleucine 199 as a strctural determinant for the selective inhibition of human monoamine oxidase B specific reversible inhibitors. *J. Biol. Chem.* **2005**, *280*, 15761−15766.) demonstrated that with rasagiline and isatin the side chain of Phe199 adopted almost identical conformations (instead of the open/closed-conformations of Ile199), without changing in either kinetics or binding affinity.
(24) Binda, C.; Li, M.; Hubàlek, F.; Restelli, N.; Edmondson, D. E.; Mattevi, A. Insights into the mode of inhibition of human mitochondrial monoamine oxidase B from high-resolution crystal structures. *Proc. Natl. Acad. Sci. U.S.A.* **2003**, *100*, 9750−9755.
(25) De Colibus, L.; Li, M.; Binda, C.; Lustig, A.; Edmondson, D. E.; Mattevi, A. Three-dimensional structure of human monoamine oxidase A (MAO A): relation to the structures of rat MAO A and human MAO B. *Proc. Natl. Acad. Sci. U.S.A.* **2005**, *102*, 12684−12689.
(26) Compound **8** was also described by Katritzky, A. R.; Akutagawawa, K. Carbon dioxide. A reagent for protection of the nucleophilic centers and the simultaneous activation of alternative locations to electrophilic attack. Part XIII. A new synthetic method for the 2-substitution of pyrrole. *OPPI* **1988**, *20*, 585−590.
(27) A different synthesis of *N*-benzyl-*N*-(1*H*-pyrrol-2-ylmethylene)amine was also published by Bandini, M.; Melloni, A.; Piccinelli, F.; Sinisi, R.; Tommasi, S.; Umani-Ronchi, A. Highly enantioselective synthesis of tetrahydro-$\beta$-carbolines and tetrahydro-$\gamma$-Carbolines via Pd-catalyzed intramolecular allylic alkylation. *J. Am. Chem. Soc.* **2006**, *128*, 1424−1425.
(28) Goa, J. A micro biuret method for protein determination. Determination of total protein in cerebrospinal fluid. Scand. *J. Clin. Lab. Invest.* **1953**, *5* 218−222.
(29) Vinter, J. G.; Davis, A.; Saunders, M. R. Strategic Approaches to Drug Design. 1. An Integrated Software Framework for Molecular Modelling. *J. Comp. Aid. Mol. Des.* **1987**, *1*, 31−55.
(30) Gasteiger, J.; Marsili, M. Iterative Partial Equilization of Orbital Electronegativity - A Rapid Access to Atomic Charges. *Tetrahedron* **1980**, *36*, 3219−3228.
(31) Hagler, A. F.; Lifson, S.; Dauber, P. Consistent Force Field Studies of Intermolecular Forces in Hydrogen-Bonded Crystals. *J. Am. Chem. Soc.* **1979**, *101*, 5122−5130.
(32) Fitzgerald, G. B.; Bauman, C.; Sajjat, Hussoin, Md.; Wick, M. Head, J. Zerner, M. C. A Broyden-Fletcher-Goldfarb-Shannon Optimization Procedure for Molecular Geometries. *Chem. Phys. Lett.* **1985**, *122*, 264−274.
(33) Bernstein, F. C.; Koetzle, T. F.; Williams, G. J. B.; Meyer, E. F., Jr.; Brice, M. D.; Rodgers, J. R.; Kennard, O.; Shimanouchi, T.; Tasumi, T. The Protein Data Bank: A Computer Based Archival File for Macromolecular Structures. *J. Mol. Biol.* **1977**, *112*, 535−542.

JM060882Y